Supporting information:

The cell size and cell size distribution of silicone rubber foams with different silica content were obtained by analyzing the SEM photographs. As Figure 1 shows, the silica content also had a strong effect on cell size distribution. The cell size distribution curve's peak shifted to the smaller cell size zone, and the cell size distribution also became narrower with an increase in the silica content.

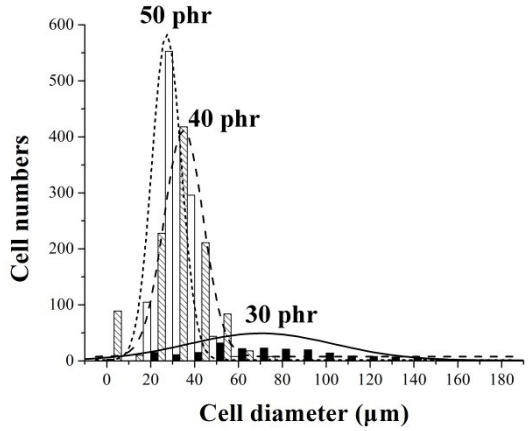

Figure 1 Statistical cell size distribution of silicone rubber foam with various silica contents.

Image analysis was further carried out on a series of foam samples to obtain the effect of the T_s on cell size distribution. The cell size and its distribution were statistically analyzed, and the results are plotted in Figure 2. When the T_s was 40 ^oC, the cell size distribution was the narrowest, and the diameter of most cells was approximately between 10~30 μm. Hence, the uniformity of cell size improved at the same time. After increasing the T_s, larger size cells formed. At 80 ^oC, the cell size distribution was the widest and the size of some larger cells was even above 100 μm.

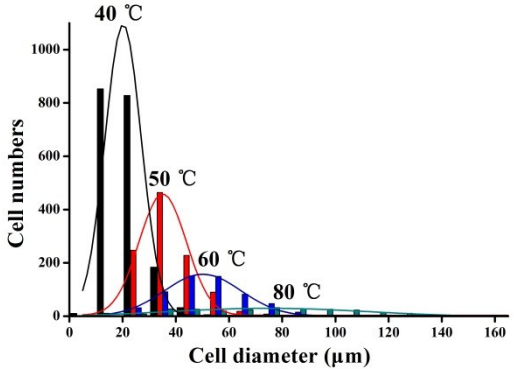

Figure 2 Statistical cell size distribution of silicone rubber foam generated at different temperatures.

The image analysis of cell size was carried out on a series of foam samples to obtain the effect of the P_s on cell structure. The cell size and its distribution were statistically analyzed and shown in Figure 15. When the P_s was 10 MPa, the cell size distribution was the widest and the diameter of most cells were distributed in the range of 40~60 μm. After increasing the P_s, the cell size distribution shifted to the left (that is, to a smaller cell size zone), and, typically, the size distribution narrowed down. The crosslinking enhances cell nucleation [43] through stress variations around the cross-linked section [41]. As a consequence, the cell density was increased with an increase in the pre-curing time.

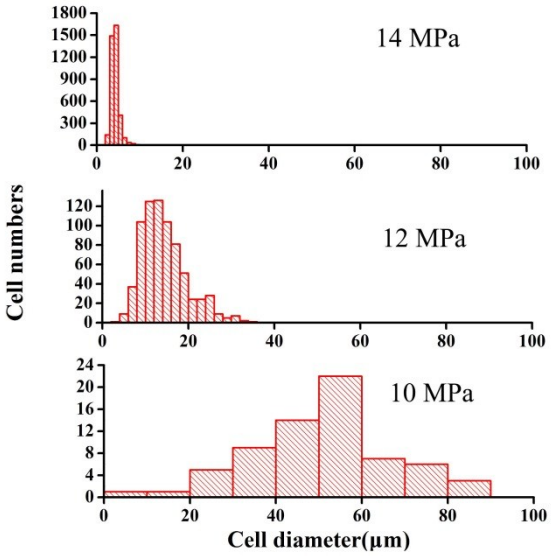

Figure 3 Statistical cell size distribution of silicone rubber foams (precuring time 18 min) generated under different pressures.

Figure 4 shows the effect of saturation temperature on the compression set of silicone rubber foams. With the increasing temperature, the compression set decreased. It is because of the lower $scCO_2$ and the increased DCP, which weaken the plasticization of CO_2.

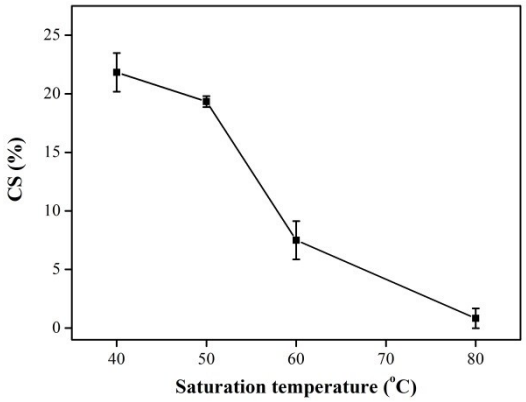

Figure 4 Effect of saturation temperature on the compression set of silicone rubber foams.

Figure 5 shows time dependence of (a) complex viscosity (η*), (b) storage (G′)

and loss (G″) modulus at a frequency of 1 Hz of silicone rubber (40 phr) at various temperatures for 1 h under atmosphere pressure. As Figure 5 shows, both the η^* and G′ of all the specimens increased but the G″ decreased during the entire testing period. It shows that DCP decomposes at all testing temperatures from 40 °C to 80 °C. This leads to increasing viscosity and promotes the formation of a cross-linked network. At the same time, the temperature also affected the motility of the molecule chains. With an increased temperature, the silicone rubber chains could move more easily, and the interaction between the silica and the rubber chains weakened. Consequently, both the η^* and G′ decreased when the temperature was increased from 40 °C to 80 °C. Considering Figure 5, it is clear that the temperature strongly enhances the motility of molecule chains, and its effect on the decomposition of the curing agent under atmospheric pressure is less.

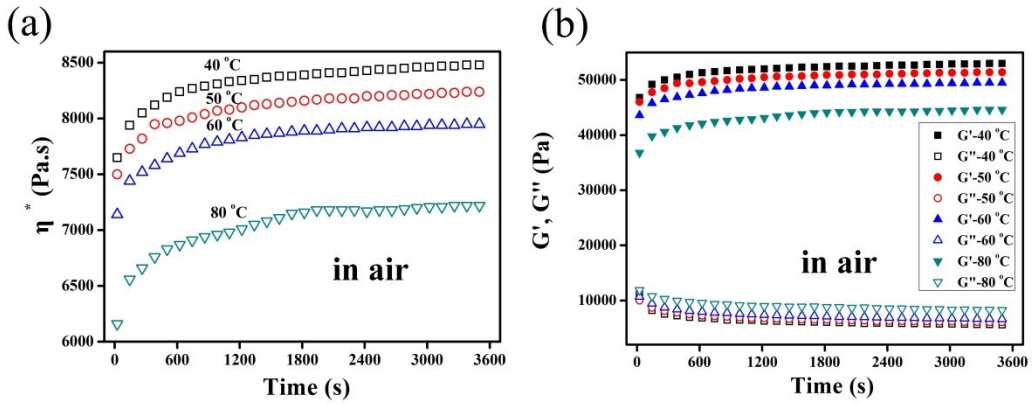

Figure 5 Time dependence of (a) complex viscosity (η^*), (b) storage (G′) and loss (G″) modulus at a frequency of 1 Hz of silicone rubber (40 phr) at various temperatures for 1 h under atmosphere pressure.